Extended Abstracts of the 2012 International Conference on Solid State Devices and Materials, Kyoto, 2012, pp993-994

Adoption of 2D-nanorod Arrays with Slanted ITO Film to Enhance Optical Asorption for Photovoltaic Applications

Yung-Chi Yao, Li-Wei She, Chun-Mao Cheng, Yi-Ching Chen, and Ya-Ju Lee*

Institute of Electro-Optical Science and Technology, National Taiwan Normal University
88, Sec.4, Ting-Chou Road, Taipei 116, Taiwan
Phone: +886-2-7734-6733 E-mail: yajulee@ntnu.edu.tw

1. Introduction

Recently, the elimination of Fresnel reflection by antireflection coatings (ARCs) has become a topic of research [1]. In particular, the development of novel ARCs that enhance the power generation efficiency of solar cells has attracted much attention. Inhomogeneous ARCs which is generally advantageous over its homogeneous counterpart because of its superior properties of broadband spectra and omnidirectional incidence [2]. However, the gradual change of refractive index in inhomogeneous ARCs must be precisely controlled during the fabrication process. Therefore, the development of novel ARCs must consider the variation of nanostructures. Herein, we report the design, implementation and demonstration of 2D Si-nanorod arrays with a slanted ITO film that shows strong absorption over a broadband spectrum (λ=400−1000nm) and a variety of incidence angles (θ=0−80°), as well as high short-circuit current density (J_{SC} =32.81 mA/cm^2) and power generation efficiency (η=22.70%).

2. Experiments and Discussion

Figure 1(a) shows a schematic of the fabrication process for the proposed ARC. In step (ii), Fig. 1(b) presents a scanning electron micrograph (SEM) of the nano-sized Ni cluster. As shown in the insert of Fig. 1(b), the diameter of an individual Ni cluster ranges from 40 to 90 nm, and exhibits a Gaussian-like distribution. On average, the diameter is approximately 60 nm. After completing the fabrication process, a continuous and porous morphology of the slanted ITO layer on the top surface was observed by SEM, as shown in Fig. 1 (c). The surface morphology of the sample was also examined by atomic force microscopy [right-hand in Fig. 1(c)]. The measured root-mean-square

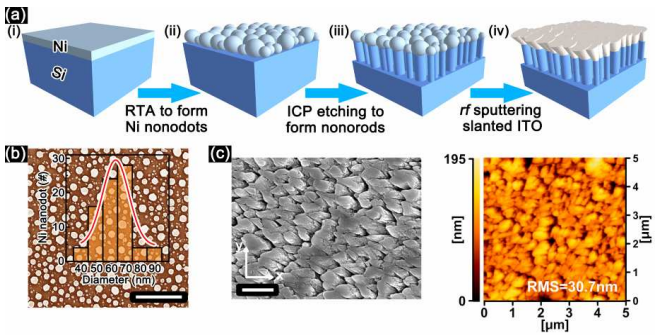

Fig. 1 (a) Schematic of the fabrication of 2D Si-nanorod array with slanted ITO film. (b) SEM image of nano-sized Ni clusters, in which the scale bare is 1μm. Insert: statistics of the diameter of distributed Ni clusters. (c) SEM (left hand) and AFM (right hand) images of the slanted ITO film grown on top of the 2D Si-nanorod array. The scale bar of the SEM image is 1 μm.

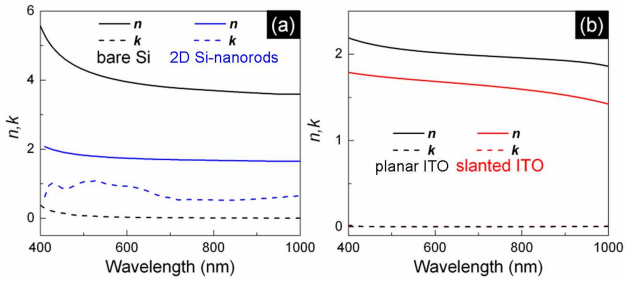

Fig. 2 Measured complex refractive indices of (a) bare Si and 2D Si-nanorod array, and (b) normal and slanted deposited ITO films by ellipsometry.

of the top surface of our ARC is about 30.7nm.

To quantitatively examine the optical characteristics of our ARC, we measured the refractive index (n) and extinction coefficient (κ) of our samples by ellipsometry, as shown in Fig. 2. Generally, the effective refractive index of the 2D Si-nanorod array can be expressed as follows [3] :

$$n_{eff}(\lambda) = n_{Si}(\lambda) + (1 - \frac{\pi D^2}{4a^2})[n_{air} - n_{Si}(\lambda)] \qquad (1)$$

where n_{Si} and n_{air} denote to the refractive indices of bare Si and the air, respectively. D is the average diameter of the 2D Si-nanorod array, a is the average pitch between

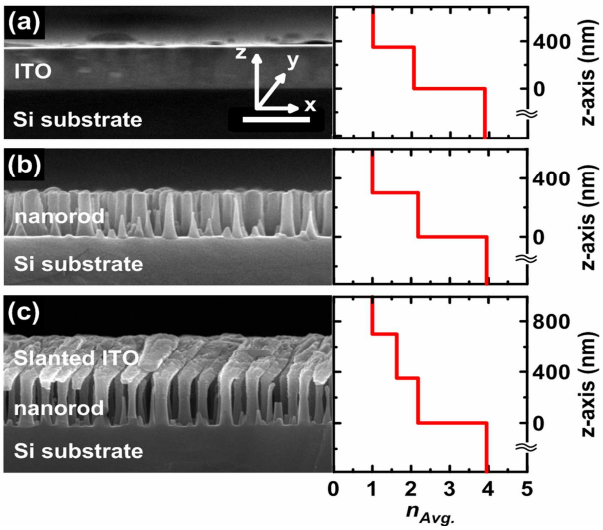

Fig. 3 Cross-sectional SEM images of (a) normally deposited ITO film, 2D Si-nanorod arrays (b) without, and (c) with the slanted ITO film. The scale bar of 500nm in the top column applies to all images. The variation of refractive index along the z-direction is also presented on the right hand side of images.

rod-to-rod, and $\pi D^2/4a^2$ is the filling-fraction (*f.f.*).

In Fig. 3, to further reduce the Fresnel reflection that occurs at its interface, we used the slanted ITO film with controllable porosity as the intermediate layer. As shown in Fig. 3(c), the slanted ITO film (d=350nm), which consists of nearly continuous nanorods with tilt angle of 40° grown by oblique-angle deposition, has a lower refractive index (n=1.68) than dense ITO (n=1.98)

Fig. 4(a) plots the measured reflectivity versus the incident wavelength. The photographs of all samples (with the identical sizes of 2cm×2cm) are also shown as inserts in the figure. Most importantly, by inserting the slanted ITO film as an intermediate layer, the measured reflectivity of 2D Si-nanorod array with slanted ITO film (blue solid line) with average value of R=9.2% is achievable over a broad spectrum.

In Fig. 4(b), the angular-dependent reflectivity of the incident wave, $R(\theta,\lambda)$, in the stack with *m* layers [inset of Fig. 4(b)] is expressed by the Airy formula as follow :

$$R(\theta,\lambda)=\left|r_{12\cdots m}\right|^2=\left|\frac{r_{12}+r_{23\cdots m}e^{-i2\varphi_2}}{1+r_{12}\cdot r_{23\cdots m}e^{-i2\varphi_2}}\right|^2 \quad (2)$$

$$r_{(m-2)(m-1)m}=\frac{r_{(m-2)(m-1)}+r_{(m-1)m}e^{-i2\varphi_{m-1}}}{1+r_{(m-2)(m-1)}\cdot r_{(m-1)m}e^{-i2\varphi_{m-1}}},\ \varphi_{m-1}=\frac{2\pi}{\lambda_0}\tilde{n}_{m-1}d_{m-1} \quad (3)$$

$$r_{(m-1)m\ \text{for TM}}=\frac{\tilde{n}_{m-1}\cos\theta_m-\tilde{n}_m\cos\theta_{m-1}}{\tilde{n}_{m-1}\cos\theta_m+\tilde{n}_m\cos\theta_{m-1}},\ \tilde{n}_m=n_m-i\kappa_m \quad (4)$$

Accordingly, the calculated results shown in Fig. 4(b) are in agreement with the measured reflectivity in Fig. 4(a).

In Fig. 4(c), the absorption ability of the samples was determined from the Airy formula for the *TM* polarized

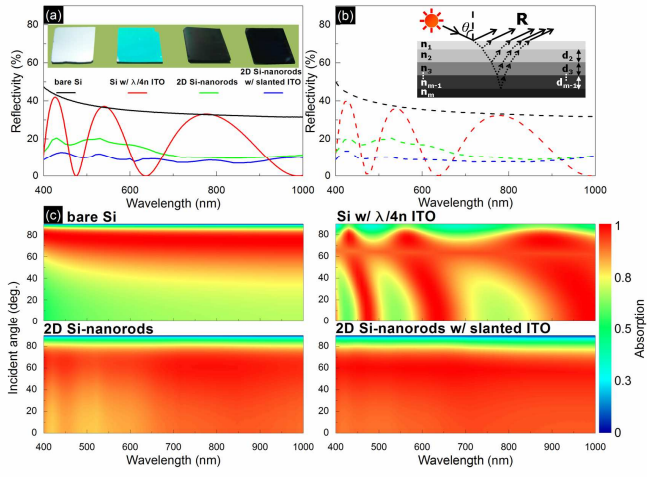

Fig. 4 (a) Measured reflectivity as a function of normal-incident wavelength for bare Si without (black solid-line) and with (red solid-line) ITO quarter-wavelength ARC, and for the 2D Si-nanorod arrays without (green solid-line) and with (blue solid-line) the slanted ITO film. Insert: photographs of the fabricated samples with dimensions of 2cm×2cm. (b) Calculated reflectivity by the Airy formula for all samples. Insert: schematic of solar light emitted into the *m*-layer stack (c) Calculated absorption, A(θ, λ), obtained by the incidence of *TM* polarized light for all samples.

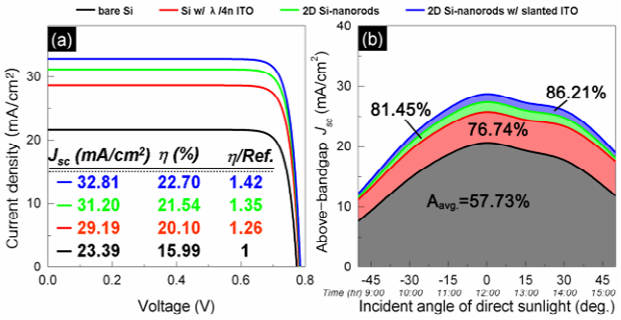

Fig. 5 (a) Calculated *J-V* curves for all samples. (b) A plot of A_{avg} calculations corresponding to each absorption $A(\theta,\lambda)$ shown in Fig. 4(c), showing the incident solar light and spectrally weighted absorption of each throughout the day.

light. Across the incident wavelengths studied here, the average absorption of the 2D Si-nanorod arrays with the addition of the slanted ITO film (θ=0−80°; λ=400−700nm) is increased to A=92.70%, and becomes nearly angle-independent over the broadband spectrum.

In Fig 5(a), The J_{SC} values of the 2D Si-nanorod arrays with slanted ITO films is 32.81 mA/cm^2. Theoretically, the V_{OC} and the *FF* of all samples are identical and remain approximately 0.8V and 0.85, respectively. As a result, a power generation efficiency of η=22.70% is achievable for the 2D Si-nanorod arrays with the slanted ITO film, corresponding to an improvement of approximately 42% with respect to that of the bare Si sample. Fig. 5(b) shows the A_{avg} calculations that correspond to the contour plot of absorption, $A(\theta,\lambda)$, shown in Fig. 4(c). Importantly, compared to that of the bare Si sample, the 2D Si-nanorod arrays with the slanted ITO films have A_{avg} = 86.21%, which corresponds to a remarkable enhancement of ~50%.

3. Conclusions

In conclusion, we have successfully demonstrated that 2D Si-nanorod arrays with slanted ITO films have strong and angle-insensitive optical absorption over a broad range of incident wavelengths and that they are advantageous for photovoltaic applications. Additionally, the results of this study concerning the optical properties of 2D nanorod arrays and slanted ITO films are not limited to Si-based solar cell, and the revealed geometry suggests techniques to produce high efficiencies in other kinds of nanoscale photovoltaic devices.

Acknowledgements

The authors gratefully acknowledge the financial support from the National Science Council of Republic of China (ROC) in Taiwan under contract Nos. NSC–100–2112–M–003–006–MY3 and NSC–100–2112–M–006–002–MY3, and from the National Taiwan Normal University under contract No. NTNU100-D-01.

References

[1] S. L. Diedenhofen, G. Vecchi, R. E. Algra, A. Hartsuiker, O. L. Muskens, G. Immink, E. P. A. M. Bakkers, W. L. Vos, and J. G. Rivas, Adv. Mater. **21** (2009) 973.

[2] S. J. Jang, Y. M. Song, C. I. Yeo, C. Y. Park, J. S. Yu, and Y. T. Lee, Opt. Express **19** (2011) A108.

[3] F. Wang, H. Y. Yu, J. Li, X. Sun, X. Wang, and H. Zheng, Opt. Lett. **35** (2010) 40.